Proceedings of the
44th IEEE Conference on Decision and Control, and
the European Control Conference 2005
Seville, Spain, December 12-15, 2005

Drag reduction by closed-loop control of a separated flow over a bluff body with a blunt trailing edge

Lars Henning and Rudibert King*

Measurement and Control Group
Institute of Process and Plant Technology
Berlin University of Technology
Hardenbergstraße 36a, 10623 Berlin, Germany

Abstract— **The present investigation focuses on the drag reduction of a bluff body with a blunt trailing edge in wind tunnel experiments. Two different approaches of closed-loop control are presented. First, a robust controller based on a family of linear black-box models is designed to suppress the vortex shedding by controlling the base pressure. To reduce the conservatism of this approach, a nonlinear static pre-compensation is included. In the second approach, a model-based sensor and an extremum seeking controller are combined to determine the optimal phase of the actuation to synchronise the vortex shedding. It is shown that the synchronisation of the vortex shedding leads to a more efficient drag reduction with respect to energy.**

I. Introduction

Flow separations behind bluff bodies, such as automobiles or ships, show complex space- and time-dependent profiles. An increased aerodynamic drag of bluff bodies is a negative consequence of this flow separation.

Thus, the suppression or a desired control of separation phenomena has been addressed in the fluid dynamics community for many decades. Various passive means for bluff body flow control are well-investigated and already applied in experiments. For example, Bearman [1] shows the effect of a splitter-plate on the wake flow of a bluff body. Tanner [2] examined the drag reduction for various kinds of a spanwise modulation of the trailing edge, such as segmented, curved, and M-shaped trailing edges. Tombazis & Bearman [3] investigated the modification of vortex shedding by adding a set of wavy trailing edges to a blunt-based model. These studies show that modifications of the geometry lead to a significant drag reduction.

However, when shaping of the geometry has reached an optimum or when passive means, such as vortex generators, have positive and negative effects, active devices in open- or closed-loop control can further improve the performance. Furthermore, active control is able to adapt the actuation to a wide range of operating conditions, even in an optimal sense.

Most of the work published so far is dedicated to open-loop control. Literature surveys on feedforward flow control, including actuation mechanisms and sensor applications, are given in Fiedler & Fernholz [4], or Gad-el-Hak et al. [5]. The effect of the active base bleed for drag reduction is proved by Bearman [6]. An active control application is investigated in Kim et al. [7] by spanwise distributed forcing at the trailing edges of a two-dimensional bluff body. Here, in large eddy simulations and wind tunnel experiments a significant drag reduction together with a suppression of vortex shedding in the wake was reached in an open-loop forcing. The first real active open-loop flow control demonstration for an airplane was done 2003 with a XV-15 tilt-rotor aircraft [8].

Closed-loop flow control of bluff bodies mainly concentrates on a well established benchmark problem, the control of the flow over a circular cylinder. In Gerhard et al. [9] a model-based flow control strategy is proposed for the suppression of vortex shedding downstream a circular cylinder. A closed-loop flow control combined with a model-based sensor is applied using a Galerkin model in Tadmor et al. [10].

Experimental validations of closed-loop flow control are still rare. In Siegel et al. [11] a simple low-dimensional model is used to control the flow over a cylinder flow. Allan et al. [12] use tuning rules for the control of a generic model of an airfoil. In Henning & King [13] a robust multivariable $\mathcal{H}_\infty$-controller is used to control the spanwise reattachment length downstream of a backward-facing step. In King et al. [14] robust and adaptive controllers are compared and used to control the spanwise and the spanwise averaged recirculation length behind a backward-facing step, the lift of a generic high-lift configuration, and the pressure recovery in a diffusor flow.

Based on these experiences, the work is carried over now to bluff body control. The paper is organised as follows: The flow configuration is given in section II with a characterisation of the physical processes exploited by the active flow control. Section III describes the synthesis of a robust controller based on Quantitative Feedback Theory. The results of wind tunnel experiments are discussed as well. Application of a model-based sensor algorithm combined with an extremum seeking feedback to the control of the base pressure is given in section IV followed by a conclusion and outlook.

* Corresponding author, email: rudibert.king@tu-berlin.de, web: http://mrt.tu-berlin.de

0-7803-9568-9/05/$20.00 ©2005 IEEE

II. Flow configuration

A. General flow description

A sketch of the bluff body configuration is given in Fig. 1. Here, a two-dimensional bluff body with a blunt trailing edge is shown. Boundary layers develop on the upper and lower body surfaces. The separation points are fixed at the upper and the lower edges, respectively. Downstream the tail of the body a separation region exists. The separation region includes the recirculation zone, characterised by a negative streamwise velocity component, and the two bordering shear layers.

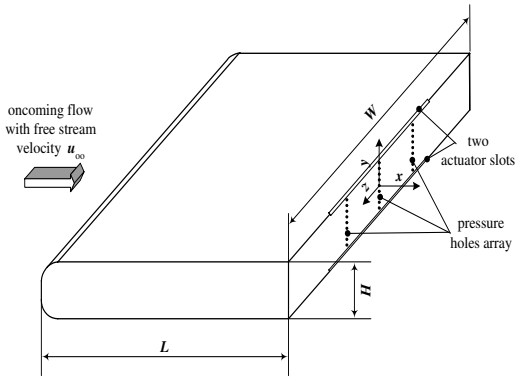

Fig. 1. Configuration of the bluff body with two actuator slots and three sensor arrays.

The two shear layers roll up into two-dimensional spanwise vortices, also called coherent structures. Due to the two-sided separation the shear layers interact. The shear layers are characterised by an alternating vortex shedding, large amplitudes of the vortices, an intensive stirring and a strong energy dissipation. The latter one is the main reason for the decrease of the pressure at the trailing edge, i.e. the base pressure. This decreased base pressure leads to an increase of the aerodynamic drag of the bluff body which is the most obvious negative effect of flow separation.

The wake flow is characterised by a dominant frequency, the so-called vortex shedding frequency f_{VS}. A non-dimensional description of this frequency is given by the Strouhal number $St_{\mathrm{H}} = f_{\mathrm{VS}}\, H/u_\infty$, where H is the body height and u_∞ is the free stream velocity.

To increase the base pressure by means of flow control, two possibilities exist. First, a suppression of the vortex shedding so that the rolling up of detrimental vortices starts father downstream. Second, a prevention of the interaction of the shear layers and a decoupling of the lower and upper vortex shedding so that less energy is dissipated.

B. Experimental set-up

The experiments are conducted in an open-type wind tunnel. The maximum free stream velocity u_∞ is $20\,\mathrm{m\,s^{-1}}$ and the turbulence level is less than 0.5%. The test section is $2500 \times 555 \times 550\,\mathrm{mm^3}$ in the streamwise (x), transverse (y) and spanwise (z) direction, respectively. The longitudinal section (xy-plane) of the bluff body corresponds with the longitudinal section of a model vehicle with a slant angle of 0° proposed by Ahmed et al. [15]. The chord length L, the height H and spanwise size W of the body are 262, 72, 550 mm, respectivly. It is mounted on two aluminium rods. The bluff body is positioned in the test section, so that the point of origin of the coordinate system is located at the centre of the test section height and 1000 mm downstream of the test section inlet.

For actuation, spanwise slots with a width of s = 1 mm and a spanwise length of 250 mm are placed at the upper and lower edges with an angle of 45° to the streamwise direction. The slots are connected with individually controllable loudspeakers. Harmonic actuations $a(t) = A(t)\sin(\omega_{\mathrm{act}}(t)\,t)$, with actuation amplitude $A(t)$ and actuation frequency $\omega_{\mathrm{act}}(t)$ are applied for each slot. This leads to a periodic sucking and blowing with a corresponding effective velocity $u_{\mathrm{act,rms}}$ at the slots. The non-dimensional momentum coefficient $c_\mu(t)$ is used to characterise the actuation amplitude in the form $c_\mu(t) = s\,u^2_{\mathrm{act,rms}}/(H\,u^2_\infty)$.

For the measurement of the base pressure, 3×9 wall pressure holes are mounted in parallel rows on the bluff body tail. These pressure hole rows are located at z/W = -0.15, 0.0 and 0.15, respectively. The pressure holes are connected to miniature amplified low pressure sensors (PascaLine, type PCLA02X5D1), which are calibrated and temperature compensated. The operating pressure range is ±2.5 mbar. These sensors are applied to obtain the non-dimensional static pressure $c_{\mathrm{P}}(t) = 2(p(t) - p_\infty)/(\rho\,u^2_\infty)$, where $p(t)$ is the measured pressure, p_∞ is the static pressure measured in the free stream velocity and ρ denotes the density. Furthermore, four strain gauges are fixed to the two aluminium rods to obtain the non-dimensional drag coefficient $c_{\mathrm{D}}(t) = 2\,F_{\mathrm{x}}(t)/(\rho\,u^2_\infty\,A_{\mathrm{cs}})$, in which $F_{\mathrm{x}}(t)$ is the measured force in streamwise direction and A_{cs} is the bluff body cross section area.

The experiments are carried out at a body height based Reynolds number $Re_{\mathrm{H}} = u_\infty\ H/\nu = 4 \times 10^4$.

The controllers are implemented on a rapid prototyping hardware (dSPACE controller board 1005 PPC) with a sampling rate of 5000 Hz.

C. Open-loop control

For the characterisation of the bluff body flow, the time averaged base pressure and the time averaged drag coefficient are measured as a function of Strouhal number and the momentum coefficients $c_\mu(t)$ at both slots. Here, the actuation signals at the lower and the upper trailing edges are in phase.

Fig. 2 shows an increase of the base pressure and a decrease of the drag coefficient in the range of $0.1 \leq St_{\mathrm{H}} \leq 0.2$. Thus, an actuation frequency of St_{H} = 0.17 is chosen in the following. Actuation with the vortex shedding frequency St_{H} = 0.25 leads to a significant decrease of the base pressure and an increase of the drag coefficient.

Fig. 3 displays the power density spectra of the pressure fluctuations measured at x/L = 0.0, y/H = 0.4 and z/W = 0.0 for the non-actuated and the actuated flow, respectively. In the case of unactuated flow, there exists a peak at St_{H} =

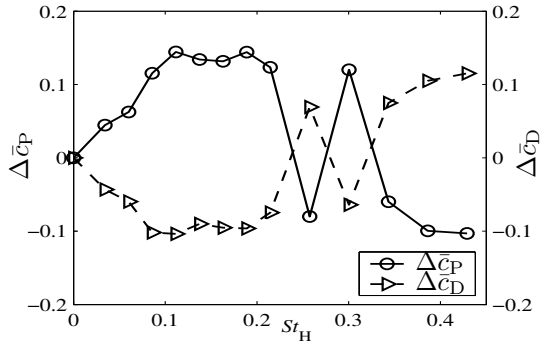

Fig. 2. Time averaged base pressure $\bar{c}_P$ and time averaged drag coefficient $\bar{c}_D$ compared to values of the unactuated case, respectively, as functions of Strouhal number St_H at $Re_H = 4 \times 10^4$ and $c_\mu = 4 \times 10^{-3}$.

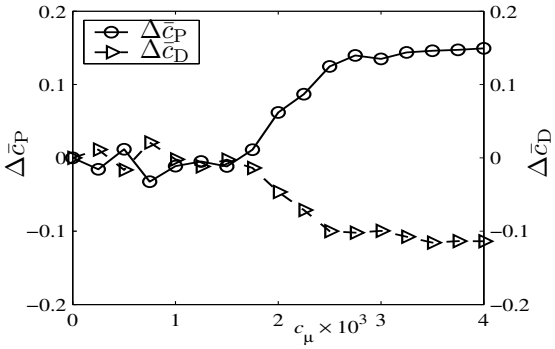

Fig. 4. Time averaged base pressure $\bar{c}_P$ and time averaged drag coefficient $\bar{c}_D$ compared to values of the unactuated case, respectively, as functions of the momentum coefficients c_μ at $Re_H = 4 \times 10^4$ and $St_H = 0.17$.

0.25 corresponding to the vortex shedding frequency. This is in good agreement with the value obtained by BEARMAN [1]. In the case of an actuated flow, a significant suppression of the vortex shedding frequency can be observed in the spectrum. The two sharp peaks at $St_H = 0.17$ and at $St_H = 0.34$ correspond to the chosen actuation frequency and its first harmonics.

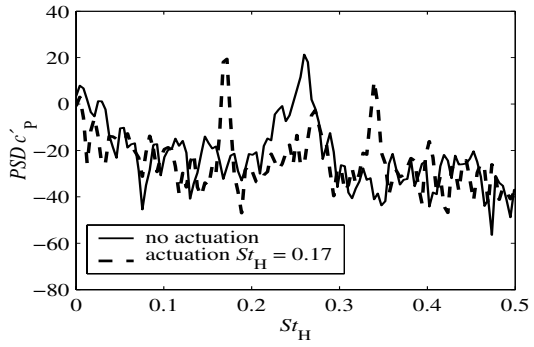

Fig. 3. Energy spectra of the pressure fluctuations measured at $x/L = 0.0$, $y/H = 0.4$ and $z/W = 0.0$ for unactuated and actuated flow at $Re_H = 4 \times 10^4$ and $c_\mu = 4 \times 10^{-3}$.

The dependence of the time averaged base pressure and the time averaged drag coefficient as a function of the momentum coefficient is given in Fig. 4. A minimum actuation energy is needed to affect the aerodynamic drag. In the range of $1.5 \times 10^3 \leq c_\mu \leq 3 \times 10^3$ an approximately linear input/output characteristic can be observed. Furthermore, the process is characterised by an output saturation. The maximum drag reduction of 0.1 corresponds to a reduction of 10 %. It should be mentioned that actuators extend to a half spanwise direction, only.

III. ROBUST CLOSED-LOOP CONTROL OF BASE PRESSURE USING QUANTITATIVE FEEDBACK DESIGN

A. Controller synthesis

To identify linear black-box models, step experiments are performed in which the momentum coefficient $c_\mu(t)$ is switched from zero to different levels at $Re_H = 4 \times 10^4$ and a constant Strouhal number of $St_H = 0.17$. Here, the spatially averaged base pressure $\bar{c}_P(t)$ is used as the output variable and the momentum coefficient $c_\mu(t)$ is chosen as the control input. A family of linear time-continuous SISO models of first order with a time delay is identified by the application of prediction error methods. The non-linearity of the investigated bluff body flow causes a wide spreading of the model parameters. Hence, the model $G(s)$ on which the robust controller synthesis is based, is described by

$$G(s) = \frac{K}{1 + T_1 s} e^{-T_0 s}$$

with the uncertain parameters $K = 0.77(1 + 0.50\Delta)$, $T_1 = 0.26(1+0.85\Delta)$ and $T_0 = 0.11(1+1.00\Delta)$, where Δ is any real scalar satisfying $|\Delta| \leq 1$.

Analysing the identified linear model family, a correlation between the momentum coefficient used for the step experiments and the values of the static gain can be found. This dependency can be fitted by a static map $f(u)$. With the inverse of this map the uncertainty of the models can be compensated to some extend. The inverse of $f(u)$ is implemented in the closed-loop as a pre-compensator, as shown in Fig. 5.

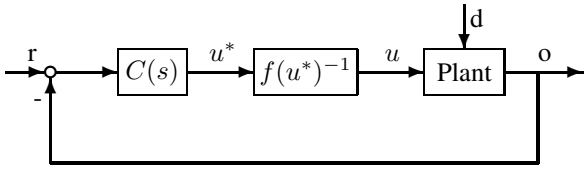

Fig. 5. Control-loop with pre-compensator ($C(s)$ - controller, r - reference, u - manipulated variable, d - disturbances, o - output).

For uncertain systems many mature controller synthesis methods do exist. Here, Quantitative Feedback Design is chosen. The important features of the approach, using the Quantitative Feedback Theory (QFT), are: (i) it is robust to the exact amount of plant uncertainty; (ii) it tailors the closed-loop precisely to the specifications which are given at each frequency; and (iii) the technique is graphically based, therefore allowing for insight into trade-offs amongst

design parameters such as amount of uncertainty, margins and bandwidth. For more details about Quantitative Feedback Theory the reader is referred to YANIV [16].

To design a controller $C(s)$, frequency domain specification are chosen on gain margin and phase margin, on sensitivity reduction and on control effort. These specifications are described in terms of inequalities on the system transfer functions as follows:

$$\begin{aligned}\left|\frac{G_0(s)}{1+G_0(s)}\right| &\leq W_1 = 1.2\\ \left|\frac{1}{1+G_0(s)}\right| &\leq W_2 = 2\\ \left|\frac{C(s)}{1+G_0(s)}\right| &\leq W_3 = 1\end{aligned}$$

where $G_0(s)$ is the open loop transfer function.

A $PIDT_1$-controller is the result of such a controller synthesis. Fig. 6 shows the Nichols plot of the nominal open-loop system $C(s)G_N(s)$ and the calculated bounds based on the specifications for some frequencies.

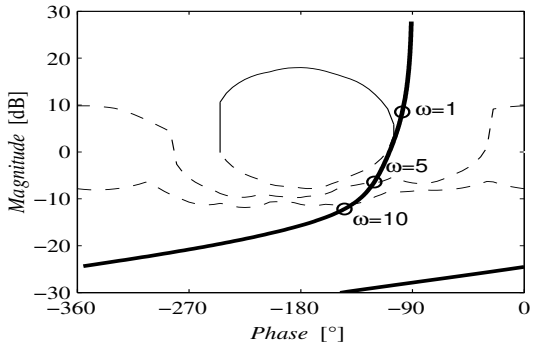

Fig. 6. Nichols plot with nominal open-loop system and calculated bounds based on closed-loop specifications for ω = 1, 5, 10 rad s^{-1}.

B. Experimental results of the robust closed-loop control

By using the robust controller synthesized with Quantitative Feedback Design the behaviour of the controlled system is tested in wind tunnel experiments with respect to tracking response and disturbance rejection.

Fig. 7 shows the tracking response of the closed-loop control after stepwise changes of the reference command. A good tracking performance can be observed. High-frequency disturbances are not rejected because of both the system's inherent limited tracking dynamics and the requirement of robustness giving a limitation of the closed-loop performance.

A main advantage of closed-loop control in comparison to open-loop control is disturbance rejection. To demonstrate the robustness of the closed-loop control the Reynolds number is varied in a range of $2 \times 10^4 \leq Re_{\mathrm{H}} \leq 6 \times 10^4$, see Fig. 8. The reference command is set to a constant value of $\bar{c}_{\mathrm{P}}$ = -0.4. In Fig. 8 a larger control error can observed at t = 45 s caused by an upper saturation of the momentum coefficient of 5×10^{-3}.

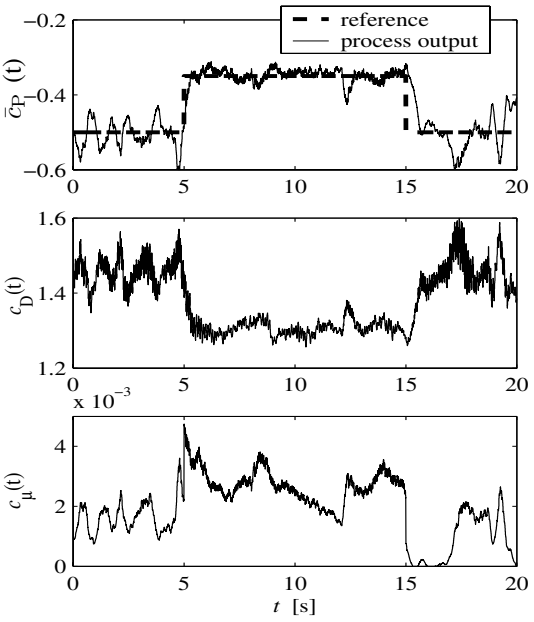

Fig. 7. Tracking response of the controlled spatial averaged base pressure (above) at Re_{H} = 4 × 10^4 and St_{H} = 0.17. Times series of drag coefficient (middle), and time series of momentum coefficient $c_\mu(t)$ acting as manipulated variable (below).

IV. EXTREMUM SEEKING CONTROL USING AN EXTENDED KALMAN FILTER

The application of the robust controller, as shown in section III, suffers from rather large values of the manipulated variable. Hence, a second approach is used here with a focus on energy saving. The idea is to reject the detrimental alternate vortex shedding and to generate a synchronized vortex shedding in the near wake, instead. Thus, the interaction of vortices is suppressed and the base pressure should increase.

A. Phase estimation

A model-based sensor algorithm which continuously estimates the wall-pressure fluctuation induced by vortex shedding at the upper trailing edge is proposed here. The Kalman filter algorithm is used for the real-time state estimation. The wall-pressure fluctuation measured at (x/L = 0, y/H = 0.4, z/W =0) can be approximated by a simple sine function $y(t) = a_0(t)\sin(\omega(t)\,t) + y_0(t)$, with the frequency $\omega(t) = 2\pi f(t)$. To use this signal for a phase control, its parameters are interpreted as states of a dynamical system. The four states are given by the frequency $f(t)$, the amplitude $a_0(t)$, the phase $\omega(t)\,t$ and an offset $y_0(t)$. The pressure fluctuations are used as information for the Kalman filter measurement update.

A simple stochastic state-space model for the description of the pressure fluctuations in discrete time is given by

$$\begin{aligned}\underline{x}(k+1) &= \begin{bmatrix}1 & 0 & 0 & 0\\ 0 & 1 & 0 & 0\\ 2\pi\Delta t & 0 & 1 & 0\\ 0 & 0 & 0 & 1\end{bmatrix}\underline{x}(k) + \underline{w}(k)\\ y(k) &= x_2(k)\sin(x_3(k)) + x_4(k)\end{aligned}$$

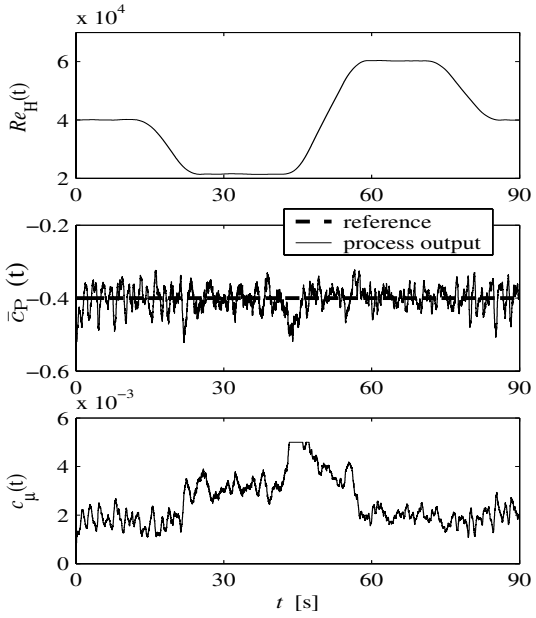

Fig. 8. Disturbance rejection of the closed-loop system (middle) during variation of the Reynolds number (above). Time series of momentum coefficient $c_\mu(t)$ as controlled variable, see below.

where Δt denotes the sampling interval and the elements of vector $\underline{w}$ are Gaussian white noises.

B. Extremum seeking feedback

A well-know control method used to achieve a maximal or minimal output of general non-linear plants with a static map is shown in Fig. 9. The extremum seeking controller consists of two filters, a low-pass filter (LP) and a high-pass filter (HP), an integrator (I), and a signal generator which supplies the controller with a harmonic sine signal $\mu\sin(\omega_\mathrm{u}t)$.

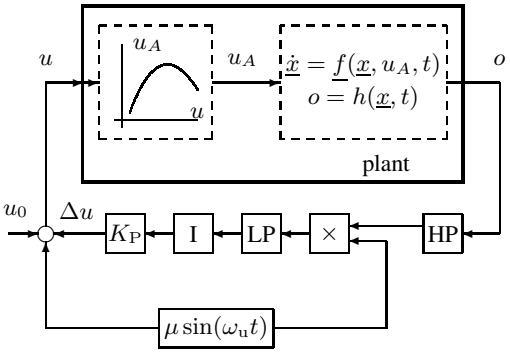

Fig. 9. Extremum seeking control (disturbances not shown) with HP - high pass, and LP - low pass filter, I - integrator, K_P - gain.

If the manipulated variable $u(t)$, i.e. the plant input, tends towards the optimal one, the output variable $o(t)$ increases, assuming that the static map has a maximum and the process dynamics are fast compared to the variation of u. The output passes through a high-pass filter which removes the mean value, but not the harmonic part with frequency ω_u. The product of the filtered output and the zero-mean sine leads to a non zero-mean signal at the output of a low pass filter as long as the maximum is not obtained. By an integration Δu is increased (or decreased) until the maximum is reached.

The choices of the gain K_P, the cut-off frequencies of the filters, the amplitude μ and the frequency ω_u of the sine signal determine the speed of convergence. The reader is referred to KRSTIC [17] for more details about extremum seeking feedback.

C. Results of extremum seeking feedback and model-based estimation

Based on the estimated states obtained by the extended Kalman filter, a harmonic actuation signal $a(t) = A(t)\sin(\omega_\mathrm{act}(t)\,t + \Delta\phi(t))$ is only applied to the lower actuator slot. $\omega_\mathrm{act}(t)$ corresponds to the estimated frequency of the upper edge, and $\Delta\phi(t)$ represents the actuation phase with respect to the phase of the upper edge vortex shedding. The actuation amplitude $A(t)$ is set to a corresponding momentum coefficient $c_\mu = 2\times10^{-3}$.

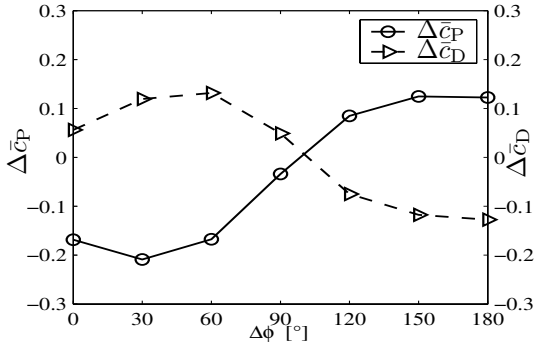

Fig. 10. Base pressure and drag coefficient as function of the phase between estimated signal and actuation signal. $Re_\mathrm{H} = 4\times10^4$, $c_\mu = 2\times10^{-3}$.

Fig. 10 shows both the time averaged base pressure and the time averaged drag coefficient as a function of the phase between the estimated and the actuated signal measured in open-loop experiments.

A significant reduction of the drag coefficient and an increased base pressure can be observed for a phase of $\Delta\phi = 180°$. Here, the actuation is out of phase. To exclude three-dimensional effects excited by actuation, the middle row of the sensor array is used for calculation of the time averaged base pressure, only.

The open-loop control strategy is expanded, so that the actuation phase is now determined by the extremum seeking feedback, i.e. the controller output $u(t)$ in Fig. 9 is the actuation phase $\Delta\phi(t)$. The plant output corresponds to the spatially averaged base pressure measured by the middle sensor row at $z/W = 0$.

The parameters of the extremum seeking controller have to be chosen appropriately. The cut-off frequencies of both the high-pass filter and the low-pass filter are set to $\omega_\mathrm{HP} = \omega_\mathrm{LP} = 1\,\mathrm{rad\,s^{-1}}$. The frequency ω_u is set equal to the cut-off frequencies of the filters. The gain is chosen as $K_\mathrm{P} = 25$.

The closed-loop performance achieved by the proposed control method is given in Fig. 11. For $0 \le t \le 10\,\mathrm{s}$

the flow is not actuated. Starting the extremum seeking at t = 10 s, initially leads to a significant decrease of the base pressure and an increase of the drag coefficient. This is the consequence of the initial actuation phase of $\Delta\phi(0) = 0°$. A maximum base pressure, however, corresponding to an increase of approximately 35%, is reached after $t \approx 20$ s. The determined actuation phase of $\Delta\phi(t)$ = -180° leads to a reduction of the aerodynamic drag of approx. 10% according to Fig. 10.

Comparing this approach with the robust closed-loop control presented in section III, this control requires approximately only half the actuation energy for equal reduction of the aerodynamic drag on the one side.

It should be mentioned, on the other side, that the applicability of this approach is restricted to a smaller Reynolds number range. Experiments with $Re_{\mathrm{H}} \geq 6 \times 10^4$ have shown that the estimation of states fails (data not shown). A decreasing amplitude of vortices with an increasing Reynolds number is the main reason. Hence, the applied pressure sensor is not able to detect pressure fluctuations induced by the vortices.

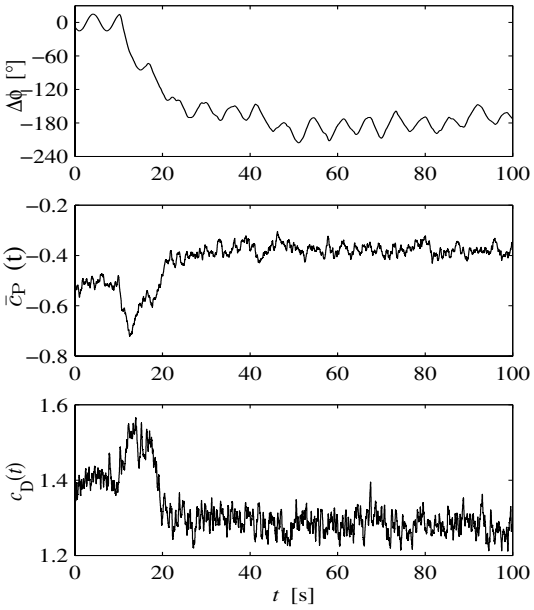

Fig. 11. Extremum seeking feedback based on an extended Kalman filter for an energy-saving reduction of aerodynamic drag. Extremum seeking starts at t = 10 s. $Re_{\mathrm{H}} = 4 \times 10^4$, $c_\mu = 2 \times 10^{-3}$.

V. Conclusion and outlook

Theses examples show that different control methods can be used for active flow control problems in experiments with regard to drag reduction. A robust controller utilises simple black-box models with a static pre-compensation of the nonlinear gain for suppression of vortex shedding in the wake flow. The methodology is particularly suitable for tracking response and disturbance rejection, as demonstrated in experiments.

An extremum seeking feedback combined with a model-based sensor is an energy-saving alternative for drag reduction. This method is based on a synchronisation of the vortex shedding in the wake flow. The success of this method is affected by the used sensor concept. A better detection of the vortex-induced fluctuations can be expected by the application of sensors with higher spatial resolution, such as wall hot-wires.

Flow visualisations, e.g. smoke visualisation or laser-Doppler anemometry (LDA), have still to be done for a better comprehension of the bluff body flow.

In the future, the applied methods will be extended to more complex three-dimensional bluff body configurations, e.g. the grounded reference car model with a base slant angle, such as the so-called 'Ahmed Body' [15].

VI. Acknowledgements

This work was founded by the German Science Foundation (DFG) as part of the Collaborative Research Centre (SFB 557) 'Control of complex turbulent shear flow'.

References

[1] P. W. Bearman, "Investigation of the flow behind a two-dimensional model with a blunt trailing edge and fitted with splitter plates," *Journal of Fluid Mechanics*, vol. 21, pp. 241–255, 1965.

[2] M. Tanner, "A method of reducing the base drag of wings with blunt trailing edges," *Aeronautical Quarterly*, vol. 23, pp. 15–23, 1972.

[3] N. Tombazis and P. W. Bearman, "A study of three-dimensional aspects of vortex shedding from a bluff body with a mild geometric disturbance," *Journal of Fluid Mechanics*, vol. 330, pp. 85–112, 1997.

[4] H.-E. Fiedler and H. Fernholz, "On management and control of turbulent shear flows," *Progress in Aeronautical Science*, vol. 27, pp. 305–387, 1990.

[5] M. Gad-el-Hak, A. Pollard, and J.-P. Bonnet, *Flow Control - Fundamentals and Practices*. Berlin, Heidelberg: Springer, 1998.

[6] P. W. Bearman, "The effect of base bleed on the flow behind a two-dimensional model with a blunt trailing edge," *Aeronautical Quarterly*, vol. 18, pp. 207–224, 1967.

[7] J. Kim, S. Hahn, J. Kim, D. Lee, J. Choi, W. Jeon, and H. Choi, "Active control of turbulent flow over a model vehicle for drag reduction," *Journal of Turbulence*, vol. 5, no. 019, 2004.

[8] I. Wygnanski, "The variables affecting the control of separation by periodic excitation," *AIAA-Paper 2004-2505*, 2004.

[9] J. Gerhard, M. Pastoor, R. King, B. Noack, A. Dillmann, M. Morzynski, and G. Tadmor, "Model-based control of vortex shedding using low-dimensional galerkin models," *AIAA-Paper 2003-4262*, 2003.

[10] G. Tadmor, B. Noack, A. Dillmann, J. Gerhard, M. Pastoor, R. King, and M. Morzynski, "Control, observation and energy regulation of wake flow instabilites," in *Proc. of the 42nd IEEE conference on decision and control 2003*, no. WeM10-4, Maui, HI, U.S.A., 2003, pp. 2334–2339.

[11] S. Siegel, K. Cohen, and T. McLaughlin, "Experimental variable gain feedback control of a cylinder wake," *AIAA-Paper 2004-2611*, 2004.

[12] B. Allan, J.-N. Juang, D. Raney, A. Seifert, L. Pack, and D. Brown, "Closed loop separation control using oscillatory flow excitation," in *ICASE-Report 2000-32*, 2000.

[13] L. Henning and R. King, "Multivariable closed-loop control of the reattachement length downstream of a backward-facing step," in *16th IFAC World Congress*, Praha, Czech Republic, July 2005.

[14] R. King, R. Becker, M. Garwon, and L. Henning, "Robust and adaptive closed-loop control of separated shear flows," *AIAA-Paper 2004-2519*, 2004.

[15] S. Ahmed, R. Ramm, and G. Faltin, "Some salient features of the time-averaged ground vehicle wake," *SAE-Paper 840300*, 1984.

[16] O. Yaniv, *Quantitative feedback design of linear and nonlinear control systems*. Kluwer Academic Publishers, 1999.

[17] M. Krstic and H.-H. Wang, "Stability of extremum seeking feedback for general nonlinear dynamic systems," *Automatica*, vol. 36, pp. 595–601, 2000.